Blind Image Restoration and Super-Resolution for Multispectral Images Using Sparse Optimization

Yoshitaka Izumi, Dan Suto, Sota Kawakami, and Hiroyuki Kudo
University of Tsukuba, Tsukuba, Japan
Email: {izumi, kawakami}@imagelab.cs.tsukuba.ac.jp, kudo@cs.tsukuba.ac.jp

Abstract—**The purpose of this paper is two-fold. First, we extend the Blind Image Deconvolution (BID) and blind Super Resolution (SR) methods developed in our previous work to multispectral images. Second, we introduce a new regularization technique called Patch-Based regularization in the BID and SR problems. This technique uses a low-rank property of image patches obtained by dividing each channel image as well as correlations in image intensity among different channels. We demonstrate performances of the proposed methods by simulation studies using images of a multispectral camera.**

Index Terms—**super-resolution, blind image deconvolution, low-rank matrix recovery**

I. Introduction

Techniques aiming at recovering an original image from single or multispectral images without knowing the Point Spread Function (p.s.f.) are called Blind Image Deconvolution (BID), and techniques aiming at recovering a high-resolution (HR) image from a Low-Resolution (LR) image without knowing the p.s.f. is called Super-Resolution (SR). The major difficulties in these problems are summarized as follows.

1) *Non-convex Nature*: When the p.s.f. is unknown, these problems lead to an optimization of a non-convex cost function, which is difficult to solve [1].
2) *Ill-posed Nature*: When the p.s.f. is unknown, these problems are inherently under-determined, because the number of unknown variables to be estimated is larger than the number of measurements [2].

Therefore, various methods have been proposed to solve these problems. In the BID problem, the major classical methods are Ayers-Dainty algorithm [3] and NAS-RIF algorithm [4]. However, it is known that the performance of these methods is not enough mainly because these methods do not overcome the two above mentioned difficulties in a successful way. In 2014, Ahmed *et al.* proposed a new method that converts the BID problem into a convex optimization, thereby leading to overcoming the issue of non-convex nature [1]. In the SR problem, there exist two major approaches. The first one is the single-frame SR, and the other is the multi-frame SR. For example, an interpolation-based method [5] and a machine-learning based method [6] belong to the category of single-frame SR. On the other hand, the multi-frame SR includes the method using multi-frame images of video sequences [7] and the motion-less SR method using multiple defocused images [8]. However, it is fair to say that most existing SR methods are assuming that the p.s.f. of camera is known.

Very recently, we have developed an improved version of Ahmed's BID method by introducing regularization terms and newest optimization techniques [9], [10]. Furthermore, we have demonstrated that this method can be applied to the problem of generating all-in-focus images as well as the blind motion-less SR problem [9], [10]. According to our knowledge, these methods work in a rather stable way compared to the classical BID techniques. However, the investigations in [9], [10] are limited to the case of single-channel image. The purpose of this paper is two-fold. First, we extend the BID and blind SR methods developed in [9], [10] to multispectral images, which are of increasing attention according to wide-spread use of multispectral cameras in a number of applications. Second, we introduce a new regularization technique called Patch-Based regularization. This technique uses a low-rank property of image patches obtained by dividing each channel image as well as correlations in image intensity among different channels. We mention that the Patch-Based regularization has been already used in several problems in image processing such as denoising and deblurring [11], [12]. We also mention that SR methods using BID have been studied by other researchers [13], [14]. However, these papers treat only the case of single-channel image.

II. Image Degradation Model

There exist various factors that degrade the measured image by using a sensor. Among them, in this paper, we consider the blurring and under sampling (down sampling), *i.e.* loss in image resolution. Such image degradation can be expressed as:

$$\vec{s} = B(\vec{f}), \vec{g} = D(\vec{s}) \tag{1}$$

Manuscript received July 25, 2021; revised November 5, 2021.

doi: 10.18178/joig.10.1.10-16

where $\vec{f}$, $\vec{s}$ and $\vec{g}$ are vectors representing the original image F, the degraded image S and the LR image G, respectively. The symbol B is a matrix representing the degradation by blurring, and D is a matrix representing the down sampling that generates the LR image from the degraded image. We consider the model given by left of Eq. (1) for the BID problem, and the model given by right of Eq. (1) for the SR problem. In Fig. 1, we show the schematic diagram of the image degradations expressed by Eq. (1).

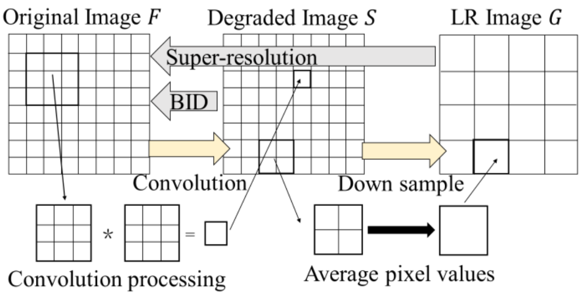

Figure 1. Image degradation models in the BID and SR problems.

III. Ahmed's Blind Image Deconvolution and Super-Resolution Methods

In this section, we review the principle of Ahmed's BID method. First, we explain fundamental mathematical knowledge used in Ahmed's BID method. The outer product $\vec{m} \otimes \vec{n}$ formed by $\vec{m}$ and $\vec{n}$, denoted by $\vec{m}\vec{n}^T$, can be expressed as:

$$\vec{m} = (m_1, m_2, \cdots, m_I)^T, \vec{n} = (n_1, n_2, \cdots, n_J)^T$$

$$\vec{m} \otimes \vec{n} = \vec{m}\vec{n}^T = \begin{pmatrix} m_1n_1 & m_1n_2 & \cdots & m_1n_J \\ m_2n_1 & m_2n_2 & \cdots & m_2n_J \\ \vdots & \vdots & \ddots & \vdots \\ m_In_1 & m_In_2 & \cdots & m_In_J \end{pmatrix} \quad (2)$$

If neither $\vec{m}$ nor $\vec{n}$ are zero vectors, the rank of matrix $\vec{m}\vec{n}^T$ is always 1. This property is used in Ahmed's BID method. Next, we describe the convolution of the image. The degradation of original image $F(x,y)$ due to the blurring is expressed by using 2-D convolution as:

$$S(x,y) = \sum_{y'=\frac{1-K_y}{2}}^{\frac{K_y-1}{2}} \sum_{x'=\frac{1-K_x}{2}}^{\frac{K_x-1}{2}} H(x',y')F(x+x',y+y') \quad (3)$$

where $S(x,y)$ is the degraded image and $H(x,y)$ is the p.s.f. of blurring. We assume that the size of both the original and blurred images is $M_x \times M_y$ (pixels), and the size of p.s.f. is $K_x \times K_y$ (pixels). The purpose of BID is to simultaneously recover $F(x,y)$ and $H(x,y)$ from only $S(x,y)$.

Hereafter, we explain Ahmed's BID method in its original form. Since Eq. (3) contains the product of $F(x,y)$ and $H(x,y)$, it is difficult to recover $F(x,y)$ and $H(x,y)$ under the condition that both $F(x,y)$ and $H(x,y)$ are unknown. This is the main reason why solving the BID problem is so difficult.

To solve the BID problem in an elegant way, Ahmed *et al.* used the following facts. First, we define the outer product matrix X formed by $\vec{f}$ and $\vec{h}$ as:

$$X = \vec{f} \otimes \vec{h} = \vec{f}\vec{h}^T \quad (4)$$

where $\vec{f}$ is the original image vector in which all elements of $F(x,y)$ are arranged according to the raster-scan order, and $\vec{h}$ is the p.s.f. vector in which all elements of $H(x,y)$ are arranged according to the raster-scan order. Since the matrix X contains products of an i-th element of $\vec{f}$ and an j-th element of $\vec{h}$ for all combinations of (i,j), Eq. (3) can be rewritten as:

$$S(x,y) = \sum_{y'=\frac{1-K_y}{2}}^{\frac{K_y-1}{2}} \sum_{x'=\frac{1-K_x}{2}}^{\frac{K_x-1}{2}} X\big((y+y')\,M_x + x + x', y'K_x + x'\big) \quad (5)$$

Therefore, using the vector $\vec{s}$ defined by arranging all elements of $S(x,y)$ according to the raster-scan order, Eq. (5) can be expressed as:

$$\vec{s} = \mathcal{A}(X) \quad (6)$$

where $\mathcal{A}$ is a linear operator that represents the image degradation due to the blurring. Here, since the matrix X is an outer product and its rank is clearly 1, Eq. (6) can be formulated as a rank minimization problem expressed as:

$$\min_X \operatorname{rank}(X) \text{ subject to } \vec{s} = \mathcal{A}(X) \quad (7)$$

However, it is well-known that the rank minimization problem is non-convex and its complexity is NP-hard. To overcome this drawback, Ahmed *et al.* replaced the rank minimization problem by the nuclear norm minimization as:

$$\min_X \|X\|_* \text{ subject to } \vec{s} = \mathcal{A}(X) \quad (8)$$

where $\|X\|_*$ denotes the nuclear norm of X. Furthermore, the same technique can be used for the SR problem, leading to:

$$\min_X \|X\|_* \text{ subject to } \vec{g} = D\big(\mathcal{A}(X)\big) \quad (9)$$

Next, we extend these formulations, *i.e.* Eq. (8) and (9), to multispectral images. During the extension, we introduce a new regularization technique by using a low-rank structure of the multi-spectral images, which is the major original contribution of this paper. We note that the use of regularization has not been described in Ahmed's original paper [1].

IV. Proposed Method

A. Formulation with Patch-Based Regularization for Multispectral Images

In this section, we first extend Eq. (8) and (9) of Ahmed's method to multispectral images. We define an outer product matrix corresponding to the n-th channel image by:

$$X_n = \overrightarrow{f_n} \otimes \overrightarrow{h_n} = \overrightarrow{f_n}\overrightarrow{h_n}^T \ (n = 1,2,\cdots,N) \quad (10)$$

where $\overrightarrow{f_n}$ and $\overrightarrow{h_n}$ are the n-th channel image vector and the n-th channel p.s.f vector, and N is the number of channels. Furthermore, we define image patches generated by dividing each channel image as:

$$Y_m = \overrightarrow{p_m} \otimes \overrightarrow{h_m} = \overrightarrow{p_m}\overrightarrow{h_m}^T (m = 1,2,\cdots,M) \quad (11)$$

where $\overrightarrow{p_m}$ and $\overrightarrow{h_m}$ are the m-th image patch vector and the p.s.f. vector, and M is the number of patches. We also define a set of all patches contained in all the channels as:

$$Y_i = Y_{\langle m\rangle n} = \overrightarrow{p_{\langle m\rangle n}} \otimes \overrightarrow{h_{\langle m\rangle n}} = \overrightarrow{p_{\langle m\rangle n}}\overrightarrow{h_{\langle m\rangle n}}^T$$

$$(n = 1,2,\cdots,N, m = 1,2,\cdots,M, i = 1,2,\cdots,NM) \quad (12)$$

We can arrange these matrices to construct a 3-rd order tensor $\mathcal{Y}$. The i-th frontal slice $Y_{::i}$ of $\mathcal{Y}$ are defined by:

$$Y_{::i} = Y_i \ (i = 1,2,\cdots,NM) \quad (13)$$

With respect to the i-th frontal slice $Y_{::i}$, Eq. (8) and (9) can be rewritten as follows, respectively.

$$\min_{Y_{::i}} \|Y_{::i}\|_* \text{ subject to } \overrightarrow{s_i} = \mathcal{A}(Y_{::i}) \quad (14)$$

$$\min_{Y_{::i}} \|Y_{::i}\|_* \text{ subject to } \overrightarrow{g_i} = D\big(\mathcal{A}(Y_{::i})\big) \quad (15)$$

$$(i = 1,2,\cdots,NM)$$

where $\overrightarrow{s_i}$ is the i-th degraded image vector and $\overrightarrow{g_i}$ is the i-th LR image vector. The formulations by Eq. (14) and (15) are simple extensions of Ahmed's BID method, where we apply Ahmed's method to each frontal slice of tensor $Y_{::i}$ separately. Finally, the method of generating a tensor $\mathcal{Y}$ from a multispectral image can be summarized as shown in Fig. 2. However, solving Eq. (14) and (15) does not provide accurate and stable solutions, because the number of unknowns to be estimated, *i.e.* the number of variables in the multi-channel image plus total number of variables in the p.s.f. $\overrightarrow{h_m}$ (m= $1,2,\cdots,M$), are much larger than the number of measured data so that the problem is underdetermined.

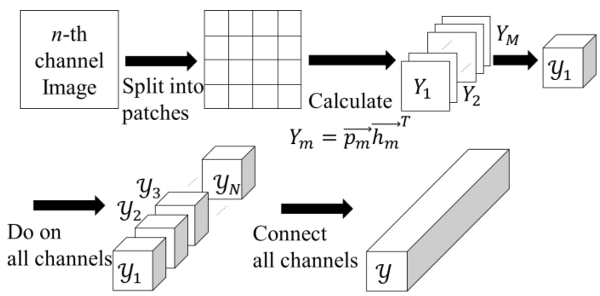

Figure 2. Illustration of how to construct a tensor.

To overcome the above difficulty, we introduce a regularization based on the low-rank property of patched multi-channel image as follows. To explain the method of regularization, we introduce the symbol "$\otimes_H$" that is defined as follows. For the tensor $\mathcal{W} \in \mathbb{R}^{X\times Y\times Z}$ and the matrices $A \in \mathbb{R}^{X\times Z}$ and $B \in \mathbb{R}^{Y\times Z}$, $\mathcal{W} = A \otimes_H B$ is defined as:

$$W_{::k} = \overrightarrow{a_k} \otimes \overrightarrow{b_k} = \overrightarrow{a_k}\overrightarrow{b_k}^T \ (k = 1,2,\cdots,Z) \quad (16)$$

Using the notation of Eq. (16) with the patch matrix $P \in \mathbb{R}^{(P_xP_y)\times(N\cdot M)}$ and the degradation process matrix $H \in \mathbb{R}^{(K_xK_y)\times(N\cdot M)}$, the tensor $\mathcal{Y}$ can be decomposed as:

$$\mathcal{Y} = P \otimes_H H \quad (17)$$

where the matrices P and H are defined by:

$$P = [\overrightarrow{p_1}, \overrightarrow{p_2}, \cdots, \overrightarrow{p_{NM}}], H = [\overrightarrow{h_1}, \overrightarrow{h_2}, \cdots, \overrightarrow{h_{NM}}] \quad (18)$$

We note that P can be interpreted as the patched multi-channel image matrix, and H can be interpreted as the collection of all p.s.f. defined for each channel n and each image patch m.

Next, we introduce regularization terms for the matrices P and H using characteristics of multi-channel images. In this work, we use the following three constraints.

1) *Similarity among Channels and Similarity among Patches*: In the multispectral images $\overrightarrow{f_n}$, different channels have similarities in image intensity. Furthermore, a set of image patch vectors $\overrightarrow{p_i} = \overrightarrow{p_{\langle m\rangle n}}$ generated by dividing each single channel image $\overrightarrow{f_n}$ into small patches $\overrightarrow{p_{\langle m\rangle n}}$ is of low-rank. Therefore, the matrix P in Eq. (18) is of low-rank.
2) *Low-rank Property of Image Matrix*: When considering a two-dimensional image as a matrix F_n, this matrix is of low-rank.
3) *Independence of p.s.f. on Channels and Patches*: The p.s.f. $\overrightarrow{h_i} = \overrightarrow{h_{\langle m\rangle n}}$ are same for all the channels $n = 1,2,\cdots,N$ and all the patches $m = 1,2,\cdots,M$.

We use Constraint 1 and Constraint 2 for the patched image matrix P and Constraint 3 for the p.s.f. matrix H. We introduce three operators $Q_1(P)$, $Q_2(P)$, and $R(H)$ to perform the regularization as follows. Since the matrix P is of low-rank (Constraint 1), the corresponding operator $Q_1(P)$ is the soft-thresholding applied to P, which is expressed as:

$$P' = Q_1(P) = S_\delta(P)$$

$$S_\delta(P) = U\mathrm{Diag}(\max\{\sigma - \delta, 0\})V^T, U\Sigma V^T = P \quad (19)$$

Next, since the matrix P contains all the pixel values of the original image, N image matrix F_n $(n = 1,2,\cdots,N)$ can be created from this matrix. Therefore, the operator $Q_2(P)$ corresponding to Constraint 2 can be constructed by the soft-thresholding acting on each F_n, which is expressed as:

$$P'' = Q_2(P); P \to F_1, F_2, \cdots, F_N$$

$$F_n' = S_\gamma(F_n) = U\mathrm{Diag}(\max\{\sigma - \gamma, 0\})V^T \quad (20)$$

$$U\Sigma V^T = F_n, P'' \leftarrow F_1', F_2', \cdots, F_N'$$

Finally, the operator $R(H)$ corresponding to Constraint 3 becomes an averaging operator which replaces all rows of the matrix H by their averages, *i.e.* taking the average of $\overrightarrow{h_1}, \overrightarrow{h_2}, \cdots, \overrightarrow{h_{NM}}$ followed by replacing all rows by the average. This operator is expressed as:

$$H' = R(H); \overrightarrow{h'_k} = \left(\overrightarrow{h_1} + \overrightarrow{h_2} + \cdots \overrightarrow{h_{NM}}\right)/(NM)$$
$$(k = 1,2,\cdots,NM) \tag{21}$$

where $\overrightarrow{h_k}$ and $\overrightarrow{h'_k}$ correspond to the matrices H and H', respectively, as in Eq. (18).

Incorporating these regularization operators into the formulations of Eq. (14) and (15), the proposed method finds a solution $\mathcal{Y} = P \otimes_H H$ to the regularized counterparts of Eqs. (14) and (15) by using an iterative algorithm based on the Proximal Gradient (PG) method similar to those used in our earlier work [9], [10]. When applied to the current multi-channel and patched problems, it consists of four steps summarized below.

(Loop to end of iterations)
[Step 1] (Update along the gradient of data fidelity term)

$$Y'_{::i} = Y_{::i} - (\tau)^{-1}\mathcal{A}^*(\mathcal{A}(Y_{::i}) - \overrightarrow{s_i}) \tag{22}$$

[Step 2] (Calculation of P', H' from $\mathcal{Y}'$ using SVD)

$$U\Sigma V^T = Y'_{::i}, \overrightarrow{p_i}' = \lambda\overrightarrow{u_1}, \overrightarrow{h_i}' = \sigma_1\overrightarrow{v_1}/\lambda \tag{23}$$

[Step 3] (Applying the constraint operators Q_1, Q_2, and R)

$$P = Q_1\left(Q_2(P')\right), H = R(H') \tag{24}$$

[Step 4] (Calculation of $\mathcal{Y}$ from P, H)

$$\mathcal{Y} = P \otimes_H H \tag{25}$$

(Go to Step 1)

In Fig. 3, we illustrate the structure of this iterative algorithm. For clarity, its more detailed form will be described in the next section.

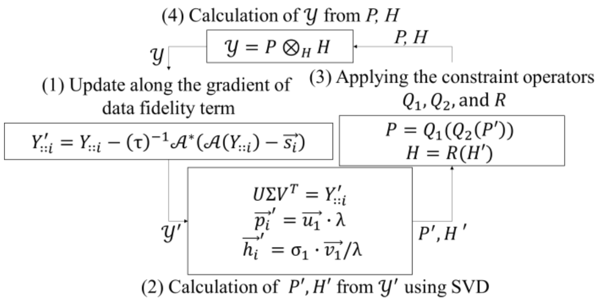

Figure 3. Structure of the proposed PG algorithm to find a solution.

B. Summary of Proposed Methods

This section describes a summary of the iterative algorithm to solve the BID problem, and the iterative algorithm to solve the SR problem. The both methods are based on the PG method. In **Algorithm 1**, we summarize the iterative algorithm to solve the regularized version of Eq. (14) based on the PG method.

Algorithm 1: Proposed BID Method

Input : $\overrightarrow{f_{n[IN]}}, \overrightarrow{h_{n[IN]}}$ $(n = 1,2,\cdots,N)$

Output : $\overrightarrow{f_{n[OUT]}}, \overrightarrow{h_{n[OUT]}}$ $(n = 1,2,\cdots,N)$

1 Calculate P^0, H^0 from $\overrightarrow{f_{n[IN]}}, \overrightarrow{h_{n[IN]}}$
  While iterating
    $k \leftarrow k + 1$
2 $\mathcal{Y}^k = P^k \otimes_H H^k$
    For all patches and channels $(i = 1,2,\cdots,NM)$
3   $Y^{k\prime}_{::i} = Y^k_{::i} - (\tau^k)^{-1}\mathcal{A}^*\left(\mathcal{A}\left(Y^k_{::i}\right) - \overrightarrow{s_i}\right)$
4   $U\Sigma V^T = Y^{k\prime}_{::i}, \overrightarrow{p^k_i}' = \lambda\overrightarrow{u_1}, \overrightarrow{h^k_i}' = \sigma_1\overrightarrow{v_1}/\lambda$
      $\left(\text{subject to sum}\left(\overrightarrow{h^k_i}'\right) = 1\right)$
    End for
5 $P^{k+1} = Q_1(Q_2(P^{k\prime})), H^{k+1} = R(H^{k\prime})$
  End while
6 Calculate $\overrightarrow{f_{n[OUT]}}, \overrightarrow{h_{n[OUT]}}$ from P^{k+1}, H^{k+1}

In **Algorithm 1**, the symbol "sum" means the sum of all elements of vector. With respect to **Algorithm 1**, we have the following remark. Normally, the PG method for nuclear norm minimization as in Eq. (14) uses the singular value thresholding operator $S_\tau(X)$ corresponding to the so-called soft-thresholding defined by Eq. (19). However, it has been reported in [9] that, under the current situation where the matrix X is of rank 1, the algorithm works much better by picking up only the maximum singular value and discarding the others. This modification significantly improves stability and convergence speed. In addition, computational cost per iteration is reduced because we need to compute only a largest singular value. In particular, in **Algorithm 1**, since it is necessary to obtain $\overrightarrow{p_i}$ and $\overrightarrow{h_i}$ from $Y_{::i}$ in each slice, we use only the singular vectors $(\overrightarrow{u_1}, \overrightarrow{v_1})$ corresponding to the maximum singular value σ_1 as in Step 4 in **Algorithm 1**.

The iterative algorithm to solve the SR problem, *i.e.* regularized version of Eq. (15), is very similar to **Algorithm 1**. The only necessary change is that Step 3 in **Algorithm 1** needs to be modified as:

$$Y^{k\prime}_{::i} = Y^k_{::i} - (\tau^k)^{-1}\left(D^*\mathcal{A}^*\left(D\left(\mathcal{A}\left(Y^k_{::i}\right)\right) - \overrightarrow{g_i}\right)\right) \tag{26}$$

where D^* is the adjoint matrix of D, and $\overrightarrow{g_i}$ is the i-th patch corresponding to the measured LR image.

V. Experimental Results

We performed experiments on the proposed BID and SR methods. The both experiments use test multispectral images distributed on Columbia University website [15]. The used multispectral images have 31 channels (bands) measured with wavelengths between 400nm and 700nm in intervals of 10nm. In implementation, we set the size of image patches to 16 (4×4) in both the experiments.

A. Simulation of Blind Image Deconvolution

First, we performed a simulation of the proposed BID method. A degraded image was generated with three different p.s.f, *i.e.* PSF1, PSF2, and PSF3. The size of all the p.s.f. are 5×5 (pixels). PSF1 is a diagonal matrix in which values of the diagonal elements are one, PSF2 is an anti-diagonal matrix in which values of the anti-diagonal elements are one, and PSF3 is a Gaussian filter where the blurring parameter was set to $\sigma = 2.0$. In Fig. 4, we illustrate the three p.s.f.

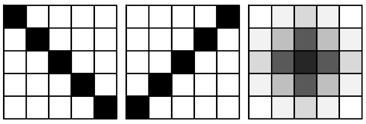

Figure 4. p.s.f. used in the simulation of BID. PSF1 (left), PSF2 (middle), and PSF3 (right).

In this experiment, values of the parameters were set to $\gamma = 1.0$ and $\delta = 5.0$ in all the p.s.f. cases. The number of iterations was 3,000. The simulation was performed by assuming that the size of p.s.f. is 7×7 (pixels). To evaluate restoration accuracy, we used the Peak-Signal-to-Noise Ratio (PSNR) and the Structural Similarity (SSIM) [16]. The value of PSNR was calculated by:

$$\mathrm{PSNR} = 20 \cdot \log_{10}\left(\frac{\mathrm{MAX}}{\sqrt{\mathrm{MSE}}}\right) \quad (27)$$

$$\mathrm{MSE} = \frac{1}{XY}\sum_{i=0}^{XY}\left(\vec{f}(i) - \vec{f'}(i)\right)^2 \quad (28)$$

where MAX denotes the maximum pixel value, $\vec{f}$, $\vec{f'}$ denote the original image and the recovered image, and Y, X denote the vertical and horizontal sizes of image. We show restored images in Fig. 5, and values of PSNR and SSIM in Table I. In Fig. 5, to save the page length, we show only the images corresponding to 21st channel. For comparison, we also show the result without regularization ($\gamma = 0.0$ and $\delta = 0.0$) and the result by the Ayers-Dainty algorithm [3] with Total-Variation (TV) [17] regularization. At the same time, we also show RGB images constructed by assigning 31st channel to R, 16th channel to G, and 6th channel to B, but we note that they are different from conventional color images taken by an RGB camera. With respect to both PSNR and SSIM, the proposed method yields the best result demonstrating that it is effective. We observe that severe artifacts appear when we use no constraints, but accurate restoration is possible when using the constraints. In addition, the Ayers-Dainty algorithm [3] with TV [17] yields relatively good results with a single image, but they cause severe artifacts in the RGB images. However, the proposed method yields good restoration results even with the RGB images by taking the channel correlation into account.

B. *Simulation of Super-Resolution*

Second, we performed a simulation of the proposed SR method. In this experiment, we used a set of LR multispectral images, which were generated by blurring HR images with p.s.f. followed by down sampling. The down sampling was done by averaging 2×2 pixel values. The parameter of Gaussian filter was set to $\sigma = 1.0$, and the size of p.s.f. was 3×3 (pixels) in PSF4 and 5×5 (pixels) in PSF5. In this experiment, values of the parameters were set to $\gamma = 1.0$ and $\delta = 5.0$ in all the p.s.f. cases, and the number of iterations was 5,000. The simulation was performed by assuming that the size of p.s.f. is 5×5 (pixels) for PSF4 and 7×7 (pixels) for PSF5, *i.e.* larger than the true support. We show restored HR images in Fig. 6, and values of PSNR and SSIM in Table II. With respect to both PSNR and SSIM, the proposed method yields the best result.

TABLE I. SUMMARY OF PSNR AND SSIM VALUES IN THE SIMULATION STUDY OF BID CASE

	Channel		Restored Image	Without Constraints	Ayers-Dainty [3]+TV	Degraded Image
PSF1	1st	PSNR	30.21	25.07	12.23	29.02
		SSIM	0.873	0.700	0.104	0.818
	21st	PSNR	22.07	17.21	14.83	20.91
		SSIM	0.734	0.519	0.293	0.589
PSF2	1st	PSNR	30.71	25.41	13.73	29.15
		SSIM	0.879	0.713	0.169	0.829
	21st	PSNR	22.12	17.29	12.40	21.68
		SSIM	0.742	0.528	0.210	0.648
PSF3	1st	PSNR	33.43	26.28	25.21	30.50
		SSIM	0.928	0.754	0.741	0.863
	21st	PSNR	23.57	18.23	17.75	21.95
		SSIM	0.765	0.515	0.431	0.652

TABLE II. SUMMARY OF PSNR AND SSIM VALUES IN THE SIMULATION STUDY OF SR CASE

	Channel		Restored Image	Without Constraints	Bicubic	Degraded Image
PSF4	1st	PSNR	33.40	23.44	32.95	30.79
		SSIM	0.940	0.666	0.920	0.877
	21st	PSNR	24.64	12.26	23.81	23.10
		SSIM	0.839	0.325	0.777	0.748
PSF5	1st	PSNR	32.23	20.92	31.81	30.22
		SSIM	0.926	0.541	0.898	0.860
	21st	PSNR	24.73	14.56	23.02	22.48
		SSIM	0.837	0.413	0.730	0.705

(a) Degraded image (b) Proposed method (c) Without constraints (d) Ayers-Dainty [3]+TV [17] (e) Original image

(a)-(e) Restored images for PSF1 (21st channel)

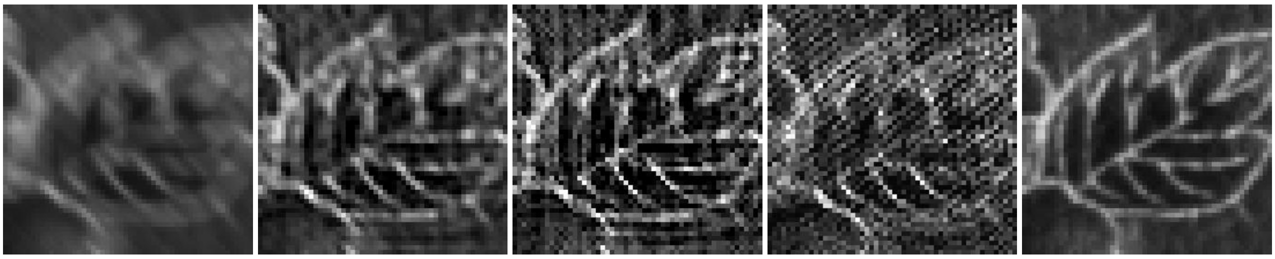

(f) Degraded image (g) Proposed method (h) Without constraints (i) Ayers-Dainty [3]+TV [17] (j) Original image

(f)-(j) PSF1 (Enlarged image of 21st channel)

(k) Degraded image (l) Proposed method (m) Without constraints (n) Ayers-Dainty [3]+TV [17] (o) Original image

(k)-(o) RGB images (Merge channels 6th, 16th, and 31st channels)

Figure 5. Restored images in the simulation of BID methods.

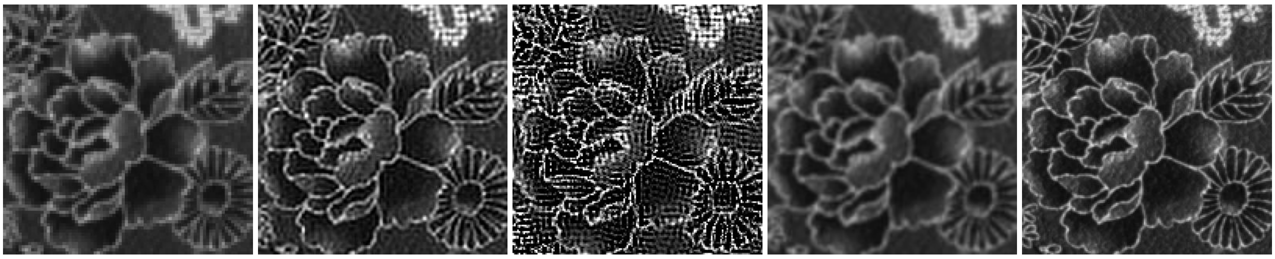

(a) LR image (b) Restored HR image (c) Without constraints (d) Bicubic (e) Original image

(a)-(e) Restored images for PSF1 (21st channel)

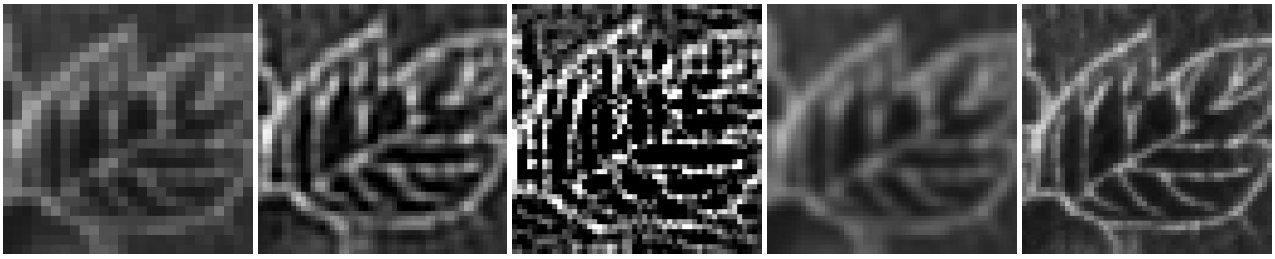

(f) LR image (g) Restored HR image (h) Without constraints (i) Bicubic (j) Original image

(f)-(j) PSF1 (Enlarged image of 21st channel)

Figure 6. Restored images in the simulation of SR methods.

VI. Conclusion

In this paper, we proposed new BID and SR methods by extending Ahmed's BID method to multispectral images and introducing Patch-Based regularization. The regularization was performed by using the channel correlation of multispectral images as well as the low-rank property of image patches in each channel image. In the experiments, we demonstrated that the proposed methods work well for both the BID and SR problems.

Conflict of Interest

The authors declare no conflict of interest.

Author Contributions

All the authors contributed to the algorithm developments. Yoshitaka Izumi, Dan Suto, and Sota Kawakami performed the implementation studies. Yoshitaka Izumi and Hiroyuki Kudo wrote the paper. All the authors approved the final version.

ACKNOWLEDGMENT

This work was partially supported by JST-CREST Project (Grant Number JPMJCR1765).

REFERENCES

[1] A. Ahmed, B. Recht, and J. Romberg, "Blind deconvolution using convex programming," *IEEE Trans. Inf. Theory*, vol. 60, no. 3, pp. 1711-1732, Mar. 2014.

[2] D. Krishnan, T. Tay, and R. Fergus, "Blind deconvolution using a normalized sparsity measure," in *Proc. CVPR*, 2011, pp. 233-240.

[3] G. R. Ayers and J. C. Dainty, "Iterative blind deconvolution method and its applications," *Opt. Lett*., vol. 13, no. 7, pp. 547-549, July 1988.

[4] D. Kundur and D. Hatzinakos, "Blind image restoration via recursive filtering using deterministic constraints," in *Proc. IEEE Int. Conf. on Acoust. Speech Signal Process*., 1996, vol. 4, pp. 2283-2286.

[5] J. V. Ouwerkerk, "Image super-resolution survey," *Image and Vision Computing*, vol. 24, no. 10, pp. 1039-1052, Oct. 2006.

[6] W. T. Freeman, T. R. Jones, and E. C. Pasztor, "Example-Based super-resolution," *IEEE Comput. Graph. Appl*., vol. 22, no. 2, pp. 56-65, Aug. 200.

[7] S. C. Park, M. K. Park, and M. G. Kang, "Super-Resolution image reconstruction: A technical overview," *IEEE Signal Process. Mag*., vol. 20, no. 3, pp. 21-36, May 2003.

[8] M. Elad and A. Feuer, "Restoration of a single superresolution image from several blurred, noisy, and undersampled measured images," *IEEE Trans. Image Process*., vol. 6, no. 12, pp. 1646-1658, Dec. 1997.

[9] S. Kawakami and H. Kudo, "All-in-Focus image generation using improved blind image deconvolution technique," in *Proc. International Conf. on Digital Medicine and Image Processing*, 2018, pp. 19-28.

[10] Y. Izumi, S. Kawakami, and H. Kudo, "Motion-Less super-resolution under blind condition using sparse optimization," in *Proc. International Conf. on Multimedia and Image Processing*, 2020, pp. 72-79.

[11] T. H. Ma, T. Z. Huang, X. L. Zhao, and Y. Lou, "Image deblurring with an inaccurate blur kernel using a group-based low-rank image prior," *Information Sciences*, vol. 408, pp. 213-233, Oct. 2017.

[12] S. Gu, L. Zhang, W. Zuo, and X. Feng, "Weighted nuclear norm minimization with application to image denoising," in *Proc. CVPR*, 2014, 2862-2869.

[13] Q. Huangpeng, X. Zeng, Q. Sun, J. Fan, J. Feng, and Z. Pan, "Super-Resolving blurry multiframe images through multiframe blind deblurring using ADMM," *Multimedia Tools and Applications*, vol. 76, pp. 13563-13579, June 2017.

[14] N. Zhao, Q. Wei, A. Basarab, N. Dobigeon, D. Kouame, and J. Y. Tourneret, "Fast single image super-resolution using a new analytical solution for l_2-l_2 problems," *IEEE Trans. Image Prosess.*, vol. 25, no. 8, pp. 3683-3697, May 2016.

[15] multispectral image database. [Online]. Available: https://www1.cs.columbia.edu/CAVE/databases/multispectral/

[16] Z. Wang, A. C. Bovik, H. R. Sheikh, and P. Simoncelli, "Image quality assessment: From error visibility to structural similarity," *IEEE Trans. Image Process.*, vol. 13, no. 4, pp. 600-612, Apr. 2004.

[17] A. Chambolle, "An algorithm for total variation minimization and applications," *Journal of Mathematical Imaging and Vision*, vol. 20, pp. 89-97, Jan. 2004.

Yoshitaka Izumi received the B.Sc. degree from the College of Information Science, University of Tsukuba, Japan, in 2019. He is a student in the Course of Computer Science, Graduate School of Systems and Information Engineering, University of Tsukuba, Japan. His major research fields are image processing and image restoration.

Dan Suto received the B.Sc. degree from the College of Media Arts, Science, and Technology, University of Tsukuba, Japan, in 2020. His major research fields are image processing and image restoration. In particular, he studied blind image restoration for multi-channel images. He received the award from the Institute of Imaging Information and Television Engineers for his research presentation on the blind image restoration.

Sota Kawakami received the B.Sc. degree from the College of Media Arts, Science, and Technology, University of Tsukuba, Japan, in 2017, and the M.S. degree from the Graduate School of Systems and Information Engineering, University of Tsukuba, Japan, in 2019. Since 2020, he is a Ph.D. student in the Degree Program in Systems and Information Engineering, Graduate School of Science and Technology, University of Tsukuba, Japan. His major research fields are image processing and image restoration.

Hiroyuki Kudo received the B.Sc. degree from the Department of Electrical Communications, Tohoku University, Japan, in 1985, and the Ph.D. degree from the Graduate School of Engineering, Tohoku University, in 1990. In 1992, he joined the University of Tsukuba, Japan. He is currently a Professor with the Division of Information Engineering, Faculty of Engineering, Information and Systems, University of Tsukuba, Japan. His research areas include medical imaging, image processing, and inverse problems. In particular, he is actively working on tomographic image reconstruction for X-ray CT, PET, SPECT, and electron tomography. He received best paper awards more than 10 times from various international and Japanese societies. He received the IEICE (The Institute of Electronics, Information, and Communication Engineers, Japan) Fellow award for his contributions on "cross-sectional image reconstruction methods in medical computed tomography". In 2018, he obtained Commendation for Science and Technology by the Minister of Education, Culture, Sports, Science and Technology for his contributions on "research on design method and image reconstruction method for new CT". For 2011-2016, he was an Editor-in-Chief of the Journal of Medical Imaging Technology (MIT). From 2020, he is a president of Japanese Society of Medical Imaging Technology (JAMIT).